80% Valley Polarization of Free Carriers in Singly Oriented Single-Layer WS_2 on Au(111)

H. Beyer,[1,*] G. Rohde,[1] A. Grubišić Čabo,[2] A. Stange,[1] T. Jacobsen,[1] L. Bignardi,[3,4] D. Lizzit,[4] P. Lacovig,[4] C. E. Sanders,[5] S. Lizzit,[4] K. Rossnagel,[1,6,7] P. Hofmann,[2] and M. Bauer[1,†]

[1]*Institut für Experimentelle und Angewandte Physik, Christian-Albrechts-Universität zu Kiel, 24098 Kiel, Germany*
[2]*Department of Physics and Astronomy, Interdisciplinary Nanoscience Center, Aarhus University, 8000 Aarhus C, Denmark*
[3]*Department of Physics, University of Trieste, 34127 Trieste, Italy*
[4]*Elettra–Sincrotrone Trieste S.C.p.A., 34149 Trieste, Italy*
[5]*Central Laser Facility, STFC Rutherford Appleton Laboratory, Harwell OX11 0QX, United Kingdom*
[6]*Ruprecht-Haensel-Labor, Christian-Albrechts-Universität zu Kiel und Deutsches Elektronen-Synchrotron DESY, 24098 Kiel und 22607 Hamburg, Germany*
[7]*Deutsches Elektronen-Synchrotron DESY, 22607 Hamburg, Germany*

(Received 23 July 2019; published 4 December 2019)

We employ time- and angle-resolved photoemission spectroscopy to study the spin- and valley-selective photoexcitation and dynamics of free carriers at the $\bar{K}$ and $\bar{K}'$ points in singly oriented single-layer WS_2/Au(111). Our results reveal that in the valence band maximum an ultimate valley polarization of free holes of 84% can be achieved upon excitation with circularly polarized light at room temperature. Notably, we observe a significantly smaller valley polarization for the photoexcited free electrons in the conduction band minimum. Clear differences in the carrier dynamics between electrons and holes imply intervalley scattering processes into dark states being responsible for the efficient depolarization of the excited electron population.

DOI: 10.1103/PhysRevLett.123.236802

Semiconducting single-layer transition metal dichalcogenides (SL TMDCs) are promising platforms for future optovalleytronic and optospintronic applications [1–4]. The remarkable properties of these materials arise from the presence of a direct band gap at the $\bar{K}$ and $\bar{K}'$ valleys in combination with a lack of structural inversion symmetry and strong spin-orbit coupling. Valley and spin degrees of freedom are strongly coupled so that a valley-selective excitation of spin-polarized carriers upon absorption of circularly polarized light becomes possible [5–8]. Experimentally, the unique properties of SL TMDCs were studied predominantly by all-optical techniques providing particular insights into the intriguing exciton physics of these materials [9–15]. For the investigation of free carrier processes it is advantageous to alternatively apply photoemission techniques, which can provide the energy, momentum, and spin sensitivity required to map out the ground and excited state electronic band structure and their properties [16–20]. The direct study of SL TMDCs by photoemission spectroscopy relies, however, on high-quality TMDC layers with typical sizes in the mm^2 regime. Bottom-up growth techniques allow for the production of such types of samples and were, for instance, successfully applied for the preparation of SL TMDCs on single crystalline noble metal substrates [21,22]. Previous angle-resolved photoemission spectroscopy (ARPES) and time-resolved ARPES (trARPES) studies of such samples revealed insights into the electronic structure and the ultrafast free carrier dynamics [21,23]. Furthermore, it was possible to demonstrate optical control of the spin and valley degrees of freedom using circularly polarized light [24]. A critical drawback of these samples is, however, the presence of mirror domains [25], which show an inversion of the $\bar{K}$ and $\bar{K}'$ points. As photoemission experiments intrinsically average over these domains, effects due to an optically induced spin and valley selectivity become reduced or completely masked. A quantitative interpretation of such data is therefore difficult or even impossible.

This Letter reports on a trARPES study of a singly oriented layer of WS_2 epitaxially grown on Au(111). The single orientation character of the sample with a maximum of 5% contribution of mirror domains was demonstrated in a comprehensive study of the structural properties [26]. This unique property makes it possible to gain quantitative information on the valley selectivity of free carrier excitation using circularly polarized light. We show that in the valence band maximum (VBM) a valley polarization of free holes of 0.84 ± 0.16 can be generated. Remarkably, the free electron valley polarization in the conduction band minimum (CBM) is lower with a value of 0.56 ± 0.16. We consider intervalley scattering processes between $\bar{K}$ and $\bar{K}'$ being responsible for this reduction, which are strongly enhanced in the CB due to an almost vanishing spin

splitting. Differences in the observed depopulation rates of excited carriers between CBM and VBM support this interpretation.

The singly oriented SL $WS_2/Au(111)$ sample was grown with a coverage of about 45% at the SuperESCA beamline of the Elettra Synchrotron radiation facility in Trieste [26]. The sample was transported to the Kiel trARPES system in an evacuated tube and cleaned by laser annealing under ultrahigh vacuum (UHV) conditions using 400 nm laser pulses ($\lesssim$50 fs pulse width) at an incident fluence of several mJ cm^{-2}. The procedure was applied until ARPES spectra of the characteristic band structure of WS_2 did not show any further changes. trARPES experiments were performed using the output of a 7.2 kHz Ti:sapphire multipass amplifier. Near-resonant excitation at the $\bar{K}$ and $\bar{K}'$ points of WS_2 was achieved at an incident fluence of $F \approx 300\ \mu$J cm^{-2} using 2.10 eV (590 nm) pump pulses generated in a noncollinear optical parametric amplifier. The polarization of the pump pulses was adjusted with a zero-order quarter-wave plate (QWP). A Stokes polarimeter was used for the quantitative characterization of the polarization state of the pulses. ARPES probe spectra were recorded with an energy resolution of 390 meV using p-polarized 22.1 eV pulses delivered from a high harmonic generation source [27] and using a hemispherical analyzer. Pump and probe pulses were focused almost collinearly at near-normal incidence onto the sample. Cross correlation measurements at the sample position yielded a time resolution of 130 fs (FWHM). All experiments were performed at a pressure of 3×10^{-10} mbar and a sample temperature of 300 K.

Figure 1(a) compares trARPES data of the sample around $\bar{K}$ before (negative pump-probe delay Δt) and during ($\Delta t = 50$ fs) the optical excitation with linearly polarized 2.10 eV pump pulses. In both spectra, one can clearly distinguish the spin-split upper and lower WS_2 valence bands (UVB and LVB) below E_F (bottom panels). Note that the states around $\bar{K}$ appear sharp and distinct and can even be used for lifetime investigations [28] due to their location in a projected bulk band gap of the Au(111) substrate, avoiding SL WS_2-substrate hybridization [22]. The additional signal at $\Delta t = 50$ fs for energies $E > E_F$ (top panels) results from the transient population of the conduction band at the CBM due to the optical excitation. Energy distribution curves (EDCs) derived from the data in Fig. 1(a) are shown in Fig. 1(b). A difference spectrum calculated from the EDCs (green line) furthermore uncovers a transient depletion of the carrier population near the UVB maximum. A finite but much weaker depletion is also visible for the LVB.

Quantitative analysis of the spectra yields a direct gap of $E_{\mathrm{gap}} = 2.06 \pm 0.07$ eV and an energy splitting between the UVB and LVB of $\Delta E_{\mathrm{VB}} = 440 \pm 70$ meV [29]. Both values are in very good agreement with earlier experiments [22,24,32] and indicate a resonant excitation between the upper VBM and CBM at the used photon energy of 2.10 eV. The observed depletion of the LVB can be associated with a transition into gap states near E_F [33,34].

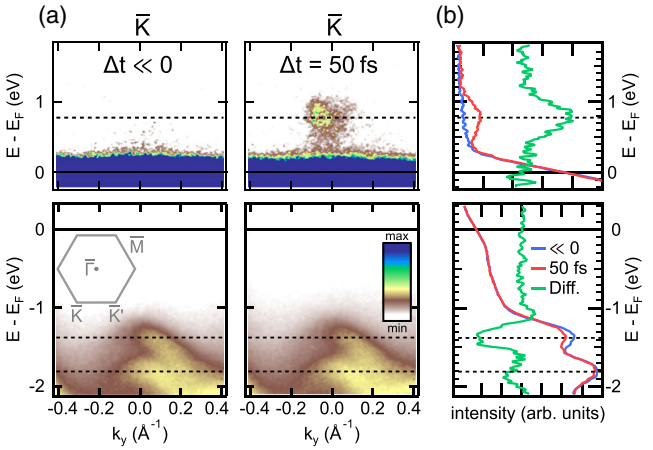

FIG. 1. Time-resolved ARPES data of $WS_2/Au(111)$ taken at $\bar{K}$ for excitation with linearly polarized 2.10 eV pump pulses. (a) ARPES snapshots recorded before optical excitation (left) and at $\Delta t = 50$ fs (right). Top (bottom) panels show the conduction (valence) band signal. Color scales have been adjusted separately for top and bottom panels to account for the significantly different photoemission intensities from CB and VB. The inset in the bottom left panel shows the hexagonal Brillouin zone of SL WS_2. (b) Comparison of energy distribution curves (EDCs) derived from the ARPES data shown in (a). Photoemission intensity was integrated over a momentum window of 0.2 Å^{-1}. The green line shows the difference calculated from the two EDCs.

A recent trARPES study of the semiconducting bulk TMDC 2H-$MoSe_2$ reported additionally on the observation of transient excitonic signatures [35]. In our case, screening due to the free carriers of the supporting gold substrate efficiently suppresses the formation of bound excitons [36]. Furthermore, the presented experiments are performed at an excitation density well above the threshold for an excitonic Mott transition in SL WS_2 [11].

Photoinduced valley selectivity within the WS_2 layer [see Fig. 2(a)] is demonstrated by comparing transient ARPES spectra at $\bar{K}$ and $\bar{K}'$) recorded 50 fs after excitation with right (σ^+) and left (σ^-) circularly polarized pump pulses, respectively. The specific delay was chosen so that the transient intensity becomes maximum. Difference intensity maps generated from these spectra are shown in Fig. 2(b). The data confirm the presence of a strong circular dichroism both in the CB and in the VB. The contrast is inverted between the $\bar{K}$ and $\bar{K}'$ points, as expected from the optical selection rules. In the VB, a dichroism is only observed in the UVB but is absent in the LVB, as can be seen particularly clearly in the difference EDCs shown in Fig. 2(c).

The experimental data presented so far confirm the qualitative findings of a related study on a SL $WS_2/Ag(111)$ sample that exhibited a preferential but not single domain orientation [24]. In the following, we will show that

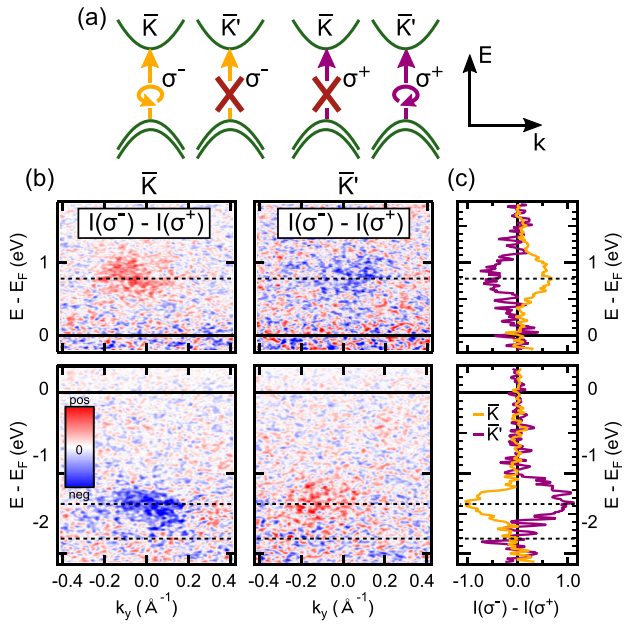

FIG. 2. Detection of valley-selective excitation of the WS_2 layer using circularly polarized light. (a) Schematic illustration of the optical selection rules of single-layer WS_2 for valley-selective excitation at $\bar{K}$ and $\bar{K}'$. (b) Difference photoemission intensity maps at $\bar{K}$ and $\bar{K}'$ obtained from trARPES spectra recorded upon excitation with σ^- and σ^+ polarized pump pulses at $\Delta t = 50$ fs. The top (bottom) panels show conduction (valence) band data. The offset of the signals with respect to $k_y = 0$ arises from the pronounced momentum dependence of the photoemission cross section of VB and CB excitation [see Fig. 1(a)]. (c) Comparison of normalized difference EDCs at $\bar{K}$ and $\bar{K}'$ derived from the data shown in (b). The signal was integrated over a momentum window of 0.35 $Å^{-1}$ and normalized to the VBM peak value.

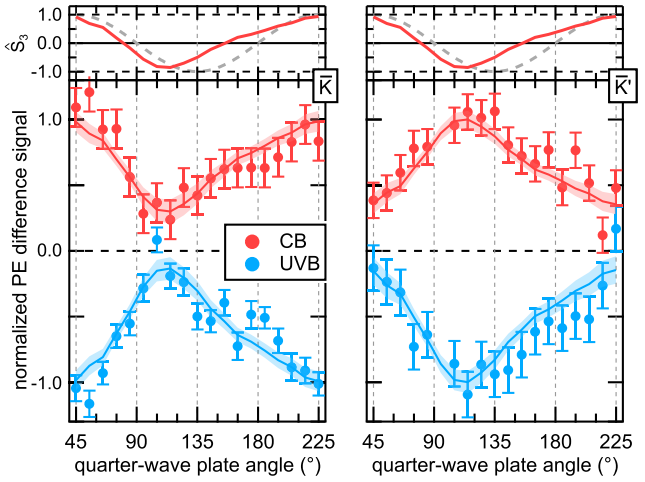

FIG. 3. Photoemission (PE) signal of CB and UVB at $\bar{K}$ and $\bar{K}'$ as a function of the angle of the quarter-wave plate in the pump beam ($\Delta t = 50$ fs). For the evaluation of the UVB data, an equilibrium state spectrum ($\Delta t \ll 0$) was subtracted from the excited state spectrum. CB (UVB) traces are normalized to maximum (minimum) PE signal. The error bars of the experimental data account for the uncertainties in determining the signal background not originating from the valley population. The solid lines are the results of the fits of Eq. (1) to the experimental data. The errors in the fits (shaded areas) account for error propagation of the fitting results and the uncertainties in determining $\hat{S}_3$. The top panel displays the normalized Stokes parameter $\hat{S}_3$ determined from the Stokes polarimeter measurements of the pump pulse [29] (red line) in comparison to an ideally polarized pump pulse (dashed gray line).

the single orientation character of our sample allows also for a quantitative determination of the valley polarization that ultimately can be generated upon optical excitation.

In the further investigations, we performed pump polarization scans with the angle of the QWP in the pump beam varied over a range of 180° in steps of 10°. The results are summarized in Fig. 3, which shows normalized integral photoemission intensities for $\Delta t = 50$ fs of the CBM (red) and the upper VBM (blue) as a function of the QWP angle. As expected for a dichroic response, we observe distinct maxima and minima as the circular polarization state is changed. The inversion of the traces at $\bar{K}$ and $\bar{K}'$ is in agreement with the valley selectivity of the excitation process shown above. Notably, the traces exhibit a clear asymmetry with respect to the QWP angle, shifting the extrema expected at 135° by approximately −20°. The polarization scan allows us to quantify the circular dichroism $D = (I_{\max} - I_{\min})/(I_{\max} + I_{\min})$ in the photoemission signal with $I_{\max}$ and $I_{\min}$ being the maxima and minima in the photoemission signal, respectively. The analysis yields circular dichroism values of $D = 0.7$ for the UVB and $D = 0.5$ for the CB. Surprisingly, the circular dichroisms in the photoemission signal from UVB and CB clearly differ.

Further quantitative analysis of the data relies on a detailed characterization of the changes in the circular polarization state of the pump pulse as the QWP angle is changed. Measurements were performed with the Stokes polarimeter and are presented and discussed in detail in the Supplemental Material [29]. The upper panels of Fig. 3 show the evaluated normalized Stokes parameter $\hat{S}_3$ of the pump pulses at the sample position as a function of the QWP angle. We observe a distinct asymmetry in the data, which can be traced back to the reflection from the final deflection mirror mounted inside the UHV chamber [29]. Additionally, the quantitative analysis of the data yields a maximum absolute value for the normalized Stokes parameter $\hat{S}_3$ of 0.9; i.e., it is not possible in this configuration to observe a circular dichroism of 100%. A comparison with the ARPES data in Fig. 3 implies that part of the observed peculiarities in the photoemission polarization scans directly reflect the circular polarization state of the pump pulse.

The Stokes polarimeter results enable us to evaluate the fraction of carriers p excited according to the optical selection rules and from this the degree of valley polarization $P = (2p - 1)$. For a given fraction f of preferentially oriented domains, the changes in the integrated

photoemission signal $I_{\bar{K}}$ at the $\bar{K}$ point during a pump polarization scan can be described by the relation [29]

$$I_{\bar{K}} \propto c \cdot f \cdot p + (1-c) \cdot (1-f) \cdot p + c \cdot (1-f) \cdot (1-p) + (1-c) \cdot f \cdot (1-p). \quad (1)$$

Here, $c = 0.5 \cdot \hat{S}_3 + 0.5$ denotes the degree of circular polarization of the pump pulse with $c = +1$ ($c = 0$) corresponding to purely σ^- (σ^+) polarized light.

The solid lines in Fig. 3 show fits of Eq. (1) to the experimental data with p being the only free fitting parameter yielding $p = 0.92 \pm 0.11$ for the UVB and $p = 0.78 \pm 0.11$ for the CB. The value for c was determined from the Stokes polarimeter data, and f was set here to $f = 1$ accounting for a perfectly oriented WS_2 layer. We conclude that upon excitation with purely circularly polarized laser pulses, an almost perfect valley-selective hole population in the UVB can be prepared. The observed value of p for the UVB results in a valley polarization $P = 0.84 \pm 0.16$. Note that in the presence of mirror domains this value can only increase. For the limiting case of a 5% contribution of mirror domains ($f = 0.95$) [26], we obtain $P = 0.94$ ($p = 0.97$). For comparison, for the valley polarization of A excitons in semiconducting SL TMDCs, theory predicts $P = 0.90$, which in this case is limited by coherent intervalley coupling [37].

The analysis of the CB data yields $P = 0.56 \pm 0.16$ ($P = 0.62$ for the limiting case of $f = 0.95$). In agreement with the observed differences in the circular dichroism, these values are significantly smaller than what we evaluated for the UVB. The analysis of time-resolved photoemission data presented in the following section provides further insights into the origin of this difference.

Figure 4(a) compares normalized photoemission intensity transients for CBM and upper VBM deduced from trARPES data at the $\bar{K}$ point with the QWP set to 45° and 135°, i.e., for excitation with predominantly σ^- and σ^+ polarized pump pulses, respectively. Note that despite the optical selection rules, we observe for both cases a finite transient signal at $\bar{K}$ due to the not perfectly circularly polarized light of the pump pulse, potential contributions from mirror domains, and a value of $p < 1$. The overall temporal evolution of the transients reflects the excited carrier population and relaxation dynamics, with the latter one being largely governed by Auger-type processes due to interaction with charge carriers in the gold substrate [23]. Notably, for the CBM, we observe clear differences in the temporal evolution for σ^+ and σ^- excitation. This implies a distinct delay in the population of the CB valley at $\bar{K}$ for the case of a predominant photoexcitation at $\bar{K}'$ (using σ^+ light). We conclude that for this excitation scenario, the CB valley at $\bar{K}'$ becomes in large part populated indirectly, and therefore delayed, by intervalley scattering from $\bar{K}'$. This indirect excitation additionally reduces the overall

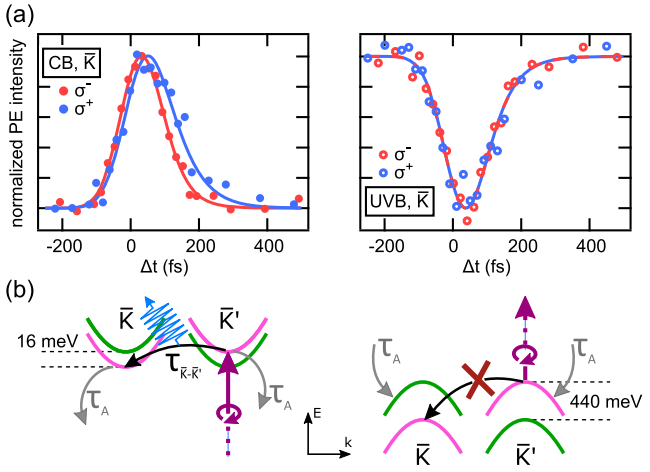

FIG. 4. Intervalley scattering of free carriers in the valence and conduction band. (a) Comparison of the temporal evolution of normalized PE intensities in the CB (left) and the UVB (right) at $\bar{K}$ for excitation with (predominantly) σ^- and σ^+ circularly polarized light. The solid lines are the results of a fit of a rate equation model to the experimental data as described in the text. For better comparison, the data are normalized to the maximum or minimum transient intensity, respectively. (b) Schematic illustration of intervalley scattering from $\bar{K}'$ to $\bar{K}$ for direct photoexcitation at $\bar{K}'$ (excitation with σ^+ circularly polarized light). Phonon emission (blue arrow) accounts for energy conservation in the intervalley scattering process in the CB. The time constants τ_A and $\tau_{\bar{K}-\bar{K}'}$ describe the decay of excited carriers according to the used rate equation model [29].

valley selectivity during the finite duration of the excitation process in our experiment. In contrast, the temporal evolution of the UVB transients remains unchanged upon switching from σ^+ to σ^- excitation. In both cases, the transient hole population in the UVB directly results from the photoexcitation process. If present at all, contributions from intervalley scattering processes are negligibly slow [38,39].

The distinct differences in the spin-orbit splitting between VB and CB, as illustrated in Fig. 4(b), can account for the differences in the observed dynamics. The small spin-orbit splitting at the CBM of only 16 meV [32] opens up spin-conserving intervalley scattering channels for photoexcited electrons from $\bar{K}'$ into the energetically lower dark states at $\bar{K}$ via phonon emission processes, as indicated by the black arrow in Fig. 4(b) [28,40]. For photoexcited holes at the upper VBM, this channel is efficiently blocked due to the large spin-orbit splitting of 440 meV, which considerably exceeds the maximum phonon energy in the system. Therefore, we propose that this spin-conserving intervalley scattering channel is responsible for the observed accelerated depopulation at the directly photoexcited CBM and the reduction in the valley polarization in the CB in comparison to the VB.

The intervalley scattering rate can be determined from a rate equation analysis of the photoemission intensity

transients of the CB and VB [29]. Fits of the rate equation model to the experimental data are added for comparison as solid lines in Fig. 4(a). The fits to the VB data yield a characteristic depopulation time constant $\tau_A = 60 \pm 20$ fs, independent of whether the direct (σ^-) or the indirect (σ^+) excitation scenario is considered. This value is in good quantitative agreement with results reported for other SL TMDCs on noble metal substrates [23,24]. The reduction of the overall lifetime compared to SL TMDCs on insulating substrates [41,42] can be associated with the population decay due to Auger-type interaction processes with carriers in the gold substrate. Assuming the same overall dynamics for CB and UVB also observed for similar sample systems [23,24], we use the same τ_A for the CB data, making the intervalley scattering time constant $\tau_{\bar{K}-\bar{K}'}$ the only free fitting parameter. These fits give a value of $\tau_{\bar{K}-\bar{K}'} = 150 \pm 50$ fs. Notably, this value agrees well with the typical timescales on the order of 100 fs predicted from theory for the formation of momentum forbidden intervalley dark excitons in W-based SL TMDCs due to electron-phonon interaction [43,44]. It should be noted that in the CB of SL WS_2 in addition to intervalley scattering processes, also phonon-mediated spin-flip intravalley scattering processes can potentially occur on very similar timescales [45]. However, due to the limited energy resolution and the lack of spin sensitivity, this type of process cannot be observed in our experiment.

In summary, our trARPES study of SL WS_2/Au(111) shows a very high valley polarization in the excited state photoemission signal. This observation confirms the absence of structural mirror domains in the studied WS_2 layer, as was shown in a previous study of the investigated sample [26]. On a closer look, we find that the valley polarization of free holes in the upper VB considerably exceeds the value for the free electrons in the CB. Substantial differences in the transient evolution of the CB intensity point to a coupling channel between $\bar{K}$ and $\bar{K}'$ that is not available for the excited carriers in the VB. This behavior can be explained by the different spin-orbit splitting of VB and CB. The herein reported valley polarization of 84% at room temperature shows that free hole excitations in SL WS_2 can be particularly attractive for future optospintronic applications.

This work was supported by the German Research Foundation through Project No. BA 2177/10-1. We gratefully acknowledge funding from VILLUM FONDEN through the Centre of Excellence for Dirac Materials (Grant No. 11744) and the Danish Council for Independent Research, Natural Sciences under the Sapere Aude program (Grant No. DFF-4002-00029).

*hbeyer@physik.uni-kiel.de
†http://www.physik.uni-kiel.de/en/institutes/bauer-group.

[1] Q. H. Wang, K. Kalantar-Zadeh, A. Kis, J. N. Coleman, and M. S. Strano, Nat. Nanotechnol. **7**, 699 (2012).
[2] S. Z. Butler *et al.*, ACS Nano **7**, 2898 (2013).
[3] X. Xu, W. Yao, D. Xiao, and T. F. Heinz, Nat. Phys. **10**, 343 (2014).
[4] K. F. Mak and J. Shan, Nat. Photonics **10**, 216 (2016).
[5] D. Xiao, G. B. Liu, W. Feng, X. Xu, and W. Yao, Phys. Rev. Lett. **108**, 196802 (2012).
[6] T. Cao, G. Wang, W. Han, H. Ye, C. Zhu, J. Shi, Q. Niu, P. Tan, E. Wang, B. Liu, and J. Feng, Nat. Commun. **3**, 887 (2012).
[7] H. Zeng, J. Dai, W. Yao, D. Xiao, and X. Cui, Nat. Nanotechnol. **7**, 490 (2012).
[8] K. F. Mak, K. He, J. Shan, and T. F. Heinz, Nat. Nanotechnol. **7**, 494 (2012).
[9] K. F. Mak, C. Lee, J. Hone, J. Shan, and T. F. Heinz, Phys. Rev. Lett. **105**, 136805 (2010).
[10] A. Splendiani, L. Sun, Y. Zhang, T. Li, J. Kim, C.-Y. Chim, G. Galli, and F. Wang, Nano Lett. **10**, 1271 (2010).
[11] A. Chernikov, C. Ruppert, H. M. Hill, A. F. Rigosi, and T. F. Heinz, Nat. Photonics **9**, 466 (2015).
[12] E. J. Sie, A. J. Frenzel, Y. H. Lee, J. Kong, and N. Gedik, Phys. Rev. B **92**, 125417 (2015).
[13] J. Yang, T. Lü, Y. W. Myint, J. Pei, D. Macdonald, J. C. Zheng, and Y. Lu, ACS Nano **9**, 6603 (2015).
[14] P. Rivera, K. L. Seyler, H. Yu, J. R. Schaibley, J. Yan, D. G. Mandrus, W. Yao, and X. Xu, Science **351**, 688 (2016).
[15] D. Christiansen, M. Selig, G. Berghäuser, R. Schmidt, I. Niehues, R. Schneider, A. Arora, S. M. de Vasconcellos, R. Bratschitsch, E. Malic, and A. Knorr, Phys. Rev. Lett. **119**, 187402 (2017).
[16] J. M. Riley, F. Mazzola, M. Dendzik, M. Michiardi, T. Takayama, L. Bawden, C. Granerød, M. Leandersson, T. Balasubramanian, M. Hoesch, T. K. Kim, H. Takagi, W. Meevasana, P. Hofmann, M. S. Bahramy, J. W. Wells, and P. D. C. King, Nat. Phys. **10**, 835 (2014).
[17] P. Hein, A. Stange, K. Hanff, L. X. Yang, G. Rohde, K. Rossnagel, and M. Bauer, Phys. Rev. B **94**, 205406 (2016).
[18] A. Bruix, J. A. Miwa, N. Hauptmann, D. Wegner, S. Ulstrup, S. S. Grønborg, C. E. Sanders, M. Dendzik, A. Grubišić Čabo, M. Bianchi, J. V. Lauritsen, A. A. Khajetoorians, B. Hammer, and P. Hofmann, Phys. Rev. B **93**, 165422 (2016).
[19] R. Wallauer, J. Reimann, N. Armbrust, J. Güdde, and U. Höfer, Appl. Phys. Lett. **109**, 162102 (2016).
[20] L. Waldecker, R. Bertoni, H. Hübener, T. Brumme, T. Vasileiadis, D. Zahn, A. Rubio, and R. Ernstorfer, Phys. Rev. Lett. **119**, 036803 (2017).
[21] S. S. Grønborg, S. Ulstrup, M. Bianchi, M. Dendzik, C. E. Sanders, J. V. Lauritsen, P. Hofmann, and J. A. Miwa, Langmuir **31**, 9700 (2015).
[22] M. Dendzik, M. Michiardi, C. E. Sanders, M. Bianchi, J. A. Miwa, S. S. Grønborg, J. V. Lauritsen, A. Bruix, B. Hammer, and P. Hofmann, Phys. Rev. B **92**, 245442 (2015).
[23] A. Grubišić Čabo, J. A. Miwa, S. S. Grønborg, J. M. Riley, J. C. Johannsen, C. Cacho, O. Alexander, R. T. Chapman, E. Springate, M. Grioni, J. V. Lauritsen, P. D. C. King, P. Hofmann, and S. Ulstrup, Nano Lett. **15**, 5883 (2015).
[24] S. Ulstrup, A. Grubišić Čabo, D. Biswas, J. M. Riley, M. Dendzik, C. E. Sanders, M. Bianchi, C. Cacho,

D. Matselyukh, R. T. Chapman, E. Springate, P. D. C. King, J. A. Miwa, and P. Hofmann, Phys. Rev. B **95**, 041405(R) (2017).

[25] O. Lehtinen, H.-P. Komsa, A. Pulkin, M. B. Whitwick, M.-W. Chen, T. Lehnert, M. J. Mohn, O. V. Yazyev, A. Kis, U. Kaiser, and A. V. Krasheninnikov, ACS Nano **9**, 3274 (2015).

[26] L. Bignardi, D. Lizzit, H. Bana, E. Travaglia, P. Lacovig, C. E. Sanders, M. Dendzik, M. Michiardi, M. Bianchi, M. Ewert, L. Buß, J. Falta, J. I. Flege, A. Baraldi, R. Larciprete, P. Hofmann, and S. Lizzit, Phys. Rev. Mater. **3**, 014003 (2019).

[27] S. Eich, A. Stange, A. V. Carr, J. Urbancic, T. Popmintchev, M. Wiesenmayer, K. Jansen, A. Ruffing, S. Jakobs, T. Rohwer, S. Hellmann, C. Chen, P. Matyba, L. Kipp, K. Rossnagel, M. Bauer, M. M. Murnane, H. C. Kapteyn, S. Mathias, and M. Aeschlimann, J. Electron Spectrosc. Relat. Phenom. **195**, 231 (2014).

[28] N. F. Hinsche, A. S. Ngankeu, K. Guilloy, S. K. Mahatha, A. Grubišić Čabo, M. Bianchi, M. Dendzik, C. E. Sanders, J. A. Miwa, H. Bana, E. Travaglia, P. Lacovig, L. Bignardi, R. Larciprete, A. Baraldi, S. Lizzit, K. S. Thygesen, and P. Hofmann, Phys. Rev. B **96**, 121402(R) (2017).

[29] See Supplemental Material at http://link.aps.org/supplemental/10.1103/PhysRevLett.123.236802 for additional information on the band positions, the Stokes polarimeter, Eq. (1), and the rate equation model, which includes Refs. [30,31].

[30] H. G. Berry, G. Gabrielse, and A. E. Livingston, Appl. Opt. **16**, 3200 (1977).

[31] B. Schaefer, E. Collett, R. Smyth, D. Barrett, and B. Fraher, Am. J. Phys. **75**, 163 (2007).

[32] P. Eickholt, C. E. Sanders, M. Dendzik, L. Bignardi, D. Lizzit, S. Lizzit, A. Bruix, P. Hofmann, and M. Donath, Phys. Rev. Lett. **121**, 136402 (2018).

[33] C. Gong, L. Colombo, R. M. Wallace, and K. Cho, Nano Lett. **14**, 1714 (2014).

[34] D. Liu, Y. Guo, L. Fang, and J. Robertson, Appl. Phys. Lett. **103**, 183113 (2013).

[35] J. H. Buss, F. Joucken, J. Maklar, H. Wang, Y. Xu, R. Unni, C. Ko, S. Tongay, J. Wu, and R. A. Kaindl, in *Conference on Lasers and Electro-Optics* (Optical Society of America, Washington, 2017), p. FTh1F.6.

[36] M. M. Ugeda, A. J. Bradley, S.-F. Shi, F. H. da Jornada, Y. Zhang, D. Y. Qiu, W. Ruan, S.-K. Mo, Z. Hussain, Z.-X. Shen, F. Wang, S. G. Louie, and M. F. Crommie, Nat. Mater. **13**, 1091 (2014).

[37] G. Berghäuser, I. Bernal-Villamil, R. Schmidt, R. Schneider, I. Niehues, P. Erhart, S. Michaelis de Vasconcellos, R. Bratschitsch, A. Knorr, and E. Malic, Nat. Commun. **9**, 971 (2018).

[38] C. Mai, Y. G. Semenov, A. Barrette, Y. Yu, Z. Jin, L. Cao, K. W. Kim, and K. Gundogdu, Phys. Rev. B **90**, 041414(R) (2014).

[39] C. Mai, A. Barrette, Y. Yu, Y. G. Semenov, K. W. Kim, L. Cao, and K. Gundogdu, Nano Lett. **14**, 202 (2014).

[40] Z. Jin, X. Li, J. T. Mullen, and K. W. Kim, Phys. Rev. B **90**, 045422 (2014).

[41] C. J. Docherty, P. Parkinson, H. J. Joyce, M.-H. Chiu, C.-H. Chen, M.-Y. Lee, L.-J. Li, L. M. Herz, and M. B. Johnston, ACS Nano **11**, 11147 (2014).

[42] P. D. Cunningham, K. M. McCreary, A. T. Hanbicki, M. Currie, B. T. Jonker, and L. M. Hayden, J. Phys. Chem. C **120**, 5819 (2016).

[43] M. Selig, G. Berghäuser, M. Richter, R. Bratschitsch, A. Knorr, and E. Malic, 2D Mater. **5**, 035017 (2018).

[44] M. Selig, G. Berghäuser, A. Raja, P. Nagler, C. Schüller, T. F. Heinz, T. Korn, A. Chernikov, E. Malic, and A. Knorr, Nat. Commun. **7**, 13279 (2016).

[45] Z. Wang, A. Molina-Sanchez, P. Altmann, D. Sangalli, D. De Fazio, G. Soavi, U. Sassi, F. Bottegoni, F. Ciccacci, M. Finazzi, L. Wirtz, A. Ferrari, A. Marini, G. Cerullo, and S. Dal Conte, Nano Lett. **18**, 6882 (2018).